



## Research Article

# Single-Cell RNA Sequencing Reveals the Interaction of Injected ADSCs with Lung-Originated Cells in Mouse Pulmonary Fibrosis

Mamatali Rahman,<sup>1,2</sup> Zhao-Yan Wang ,<sup>1,2</sup> Jun-Xiang Li,<sup>1,2,3,4</sup> Hao-Wei Xu,<sup>1,2</sup> Rui Wang,<sup>1,2</sup> and Qiong Wu <sup>1,2</sup>

<sup>1</sup>MOE Key Laboratory of Bioinformatics, Center for Synthetic and System Biology, Tsinghua University, Beijing 100084, China

<sup>2</sup>School of Life Sciences, Tsinghua University, Beijing 100084, China

<sup>3</sup>AGECODE R&D Center, Yangtze Delta Region Institute of Tsinghua University Zhejiang, Jiaxing, China

<sup>4</sup>TUS-HARVEST Biotech. Co. Ltd, China

Correspondence should be addressed to Qiong Wu; wuqiong@mail.tsinghua.edu.cn

Received 3 December 2021; Accepted 10 March 2022; Published 11 April 2022

Academic Editor: Eva Mezey

Copyright © 2022 Mamatali Rahman et al. This is an open access article distributed under the Creative Commons Attribution License, which permits unrestricted use, distribution, and reproduction in any medium, provided the original work is properly cited.

Pulmonary fibrosis (PF) is a severe chronic lung disease with little effective treatment options other than lung transplantation. Adipose-derived mesenchymal stem cells (ADSCs) have been shown to exert therapeutic effects on PF, but the underlying mechanisms remain to be further elucidated. Here, we show the interaction of ADSCs and lung-originated cells at the single-cell level, using bleomycin- (BLM-) induced mice PF model and green fluorescent protein- (GFP-) labeled mouse ADSCs. The intratracheally injected ADSCs were successfully recollecting with flow cytometry and, together with lung-originated cells, were subjected to single-cell RNA sequencing (scRNA-seq). The ADSC treatment drastically changed the transcriptomic profile and composition of lung cells, especially macrophages. We explored the signal pathway interactions between ADSCs and lung-originated cells, showing potentially regulative pathways including NGR, ANNEXIN, HGF, and PERIOSTIN. Our data indicate that the injected ADSCs increased the number of *Trem2*<sup>+</sup> antiinflammatory lung macrophages and lowered further inflammation and fibrosis in the lung. Our work realized the direct analysis of injected ADSCs to explore its *in vivo* interaction with the lung environment under PF and may provide critical information for future engineering of ADSCs to achieve better therapeutic effects in PF.

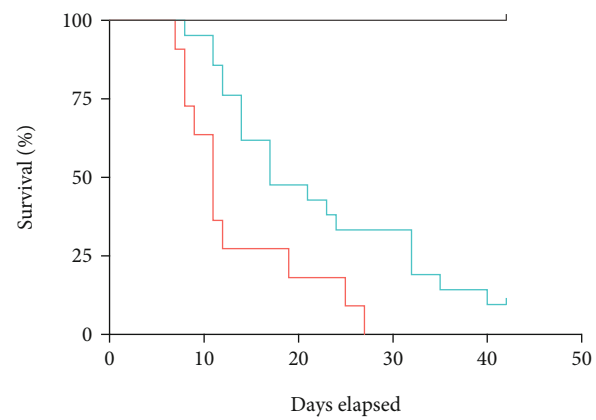
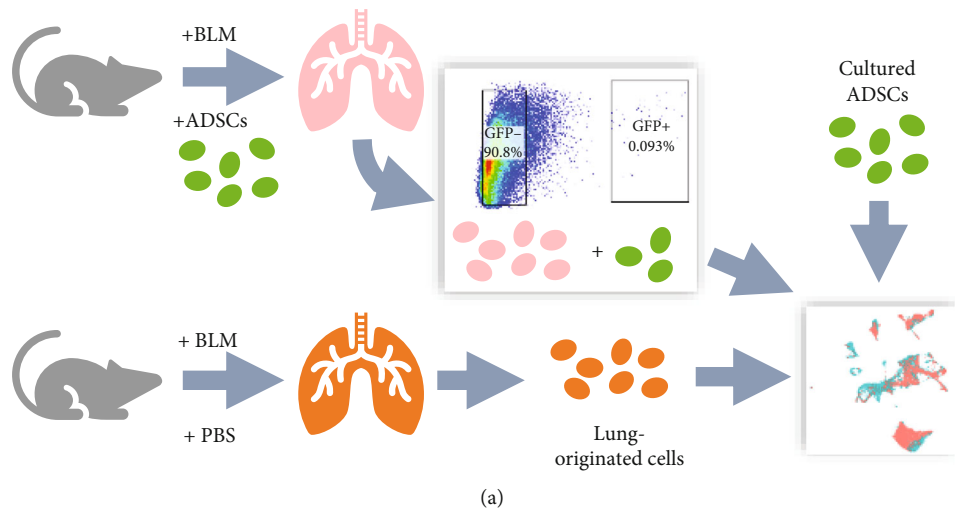
## 1. Introduction

Pulmonary fibrosis (PF) denotes a heterogeneous group of severe and lethal interstitial lung diseases, involving progressive lung remodeling, alveolar destruction, excessive pathological extracellular matrix (ECM) deposition, and scarring of the lungs [1–3]. The pathogenesis involves multiple biological pathways, including inflammatory response, apoptosis, oxidative stress, and epithelial to mesenchymal transition [4–8].

PF is traditionally considered to be an irreversible lung disease that is refractory to various treatments, resulting in high rates of mortality and morbidity [9]. Recently, the administration of mesenchymal stem cells (MSCs) has emerged as a promising therapy for PF [10, 11]. MSCs have

been isolated from various tissues such as the bone marrow, adipose tissue, and the stroma of organs. They exhibit self-renewal ability and the potential to differentiate into a variety of cell lineages, including chondrocytes, osteoblasts, and adipocytes [12, 13]. And it is reported that MSCs attenuate fibrotic diseases including PF, by immunomodulation, anti-apoptosis, antiinflammation, and antifibrosis functions [14–18]. Among several sources of MSCs, ADSCs have the advantages of easy accessibility and relative abundance, which make a practical cell source for cell therapy [19, 20].

The effects of ADSCs have been widely investigated using both *in vitro* cultures and *in vivo* models. But on one hand, direct recovery and analysis of injected ADSCs were not performed yet, likely due to in adaptation and apoptosis after entering the pathological environment [21]; on the



— PBS (n = 10)  
 — BLM + PBS (n = 22)  
 — BLM + ADSCs (n = 21)

(b)

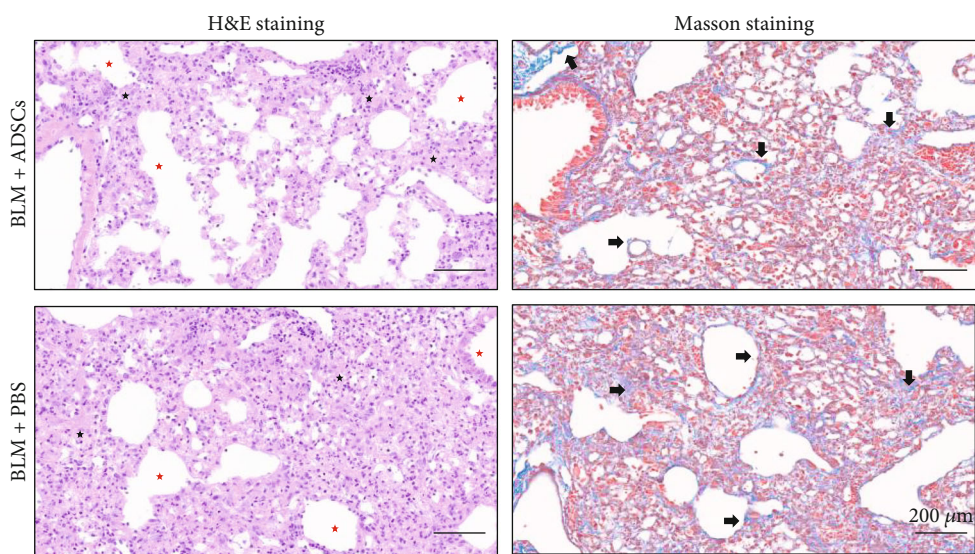


FIGURE 1: Continued.

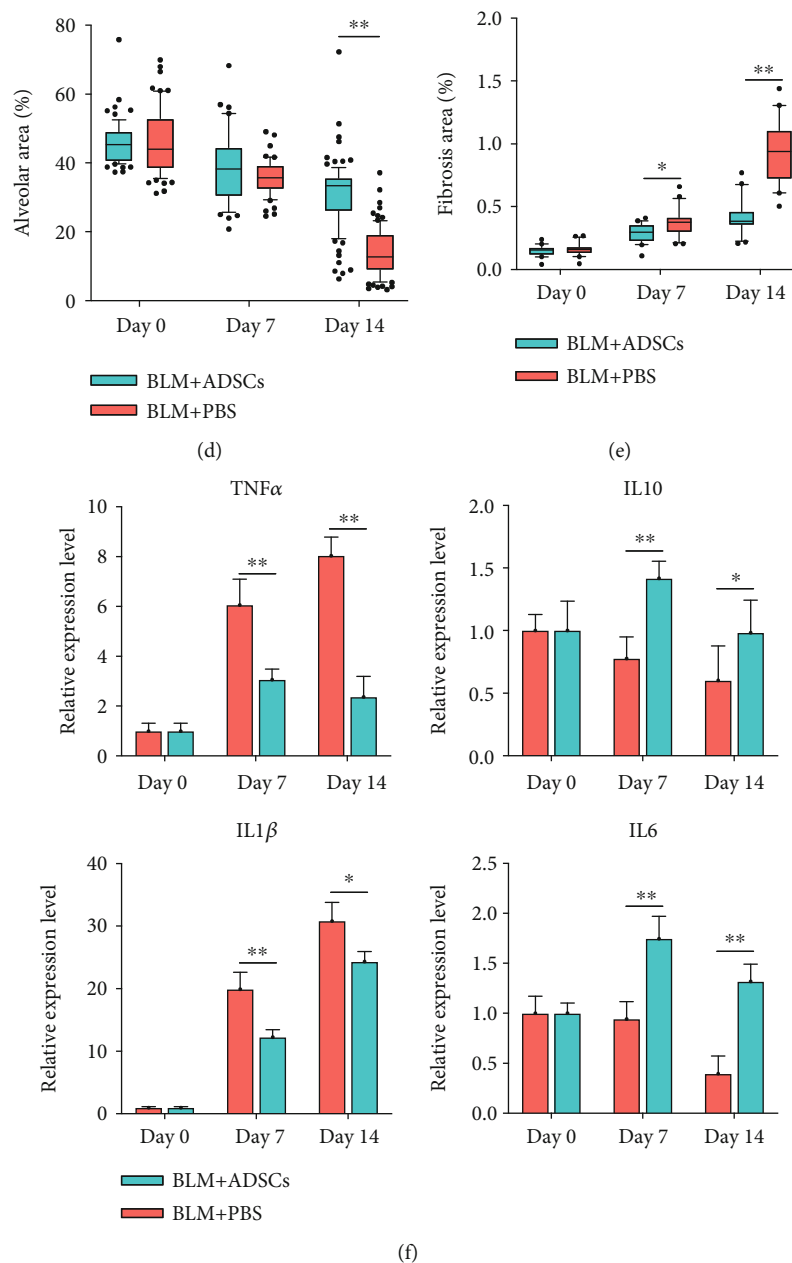


FIGURE 1: Intratracheal injection of ADSCs alleviated mouse pulmonary fibrosis. (a) The diagram of the study. (b) Kaplan-Meier survival curve for pulmonary fibrosis mice. The group was received PBS ( $n = 10$ , black line), the BLM + PBS group administered 3.5 mg/kg BLM in 50  $\mu$ l PBS at day 0 ( $n = 21$ , red line), and BLM + ADSCs group received  $5 \times 10^5$  cell in 50  $\mu$ l PBS by intratracheally at day 3 post-BLM administration. (c) Masson's and H&E staining images of the lung tissues of mice on day 14, scale bar: 200  $\mu$ m. (d) Density of pulmonary fibrotic tissue (fibrosis area (black arrow)/total area  $\times$  100%) calculated on histological sections of Masson's trichrome staining. (e) Density of the pulmonary tissue (alveolar (red star) area  $\div$  parenchyma (black star) area  $\times$  100%) calculated on histological sections of H&E trichrome staining. (f). Relative expression of TNF- $\alpha$ , IL-1 $\beta$ , IL-10, and IL-6 mRNA in the pulmonary tissue of BLM + ADSC and BLM + PBS group ( $n = 3$  each) determined by quantitative real-time polymerase chain reaction, on days 7 and 14. Data presented as mean  $\pm$  SD with significance based on Student  $t$ -test. \* $P < 0.05$ ; \*\* $P < 0.01$ .

other hand, current characterization of ADSC-treated BLM lung remains on the tissue (bulk) level, while scRNA-seq can provide a higher resolution of the therapeutic effect, as well as enabling cell-cell interaction inference from the tran-

scriptomic data. Therefore, in this study, we recollected the injected allogenic mouse ADSCs from BLM-treated mouse lungs and subjected recollected ADSCs and lung-originated cells to scRNA-seq to analyze the crosstalk

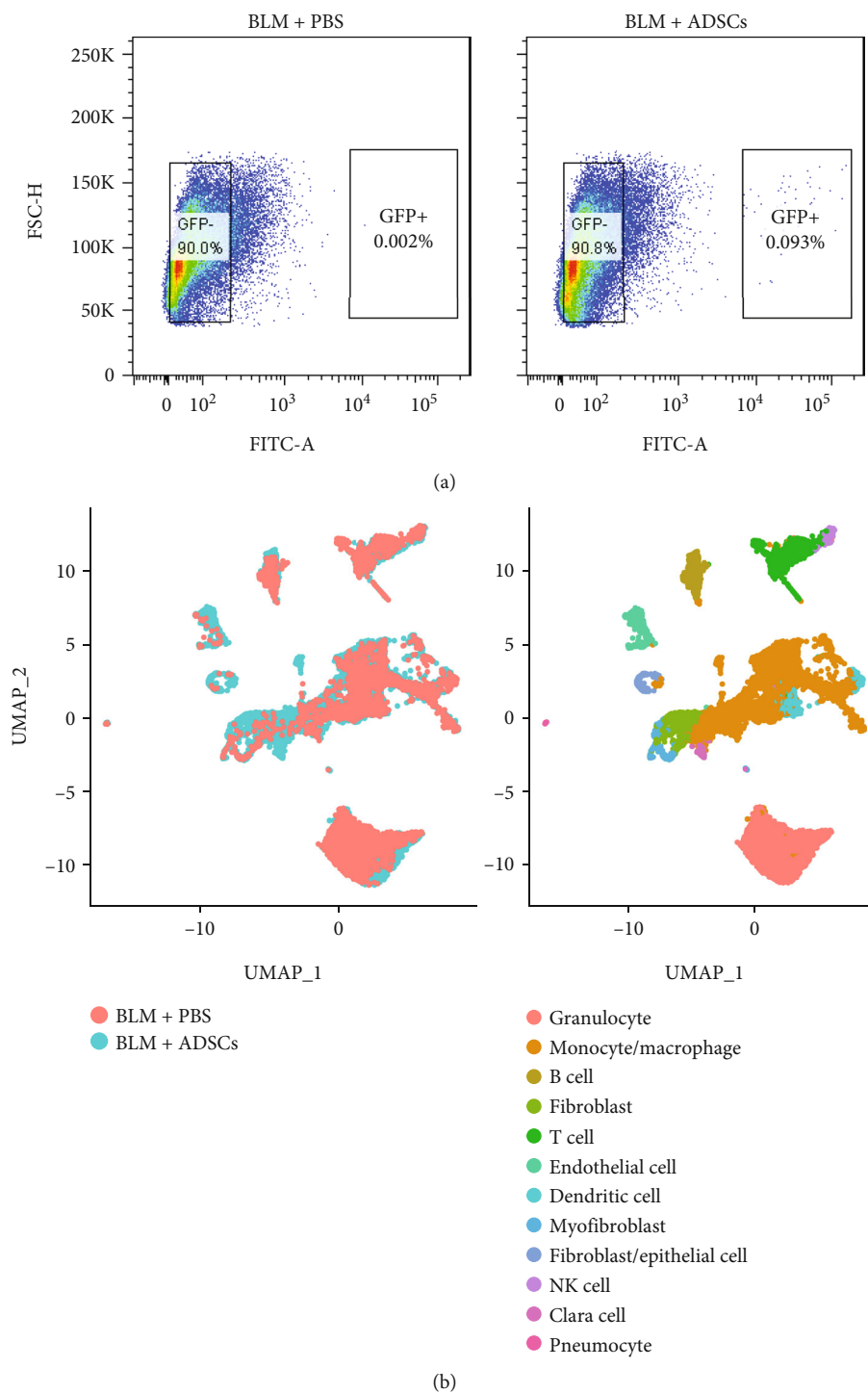
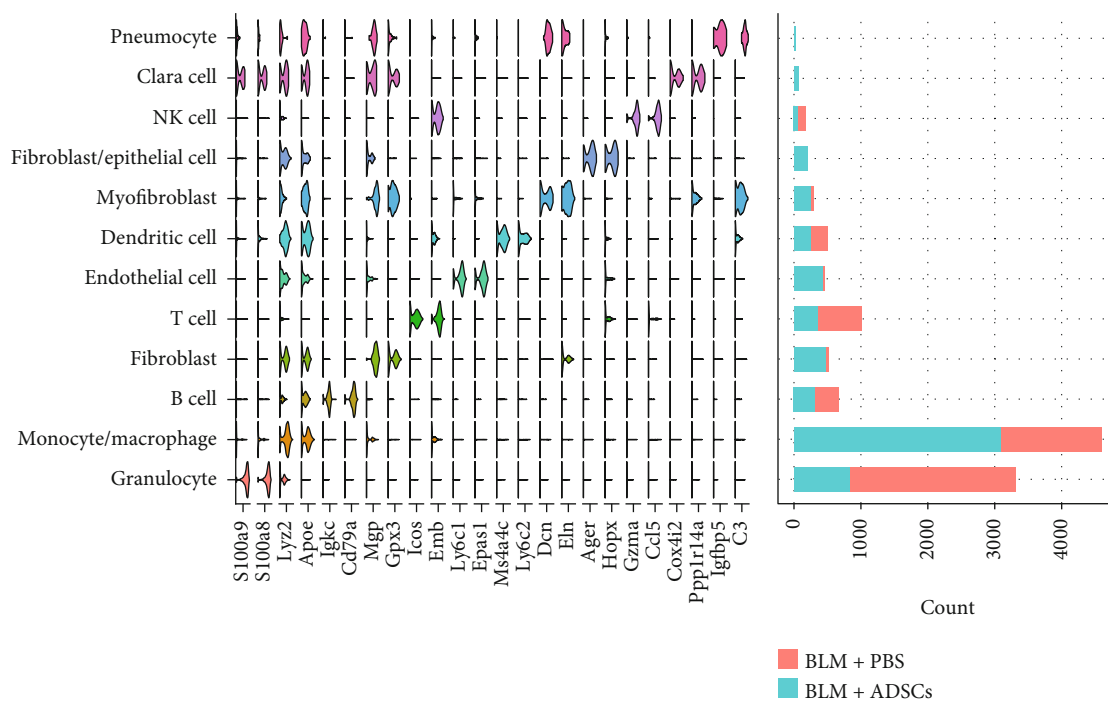


FIGURE 2: Continued.



(c)

FIGURE 2: Injected ADSCs greatly changes single-cell heterogeneity of BLM-treated lung tissue. (a) Flow cytometry diagrams for sorting of digested lung tissue based on GFP signal intensity. Left: BLM + PBS group, as non-GFP control for lung-originated cells only. Right: BLM + ADSCs group, showing a small population of GFP+ cells, which are considered recollected ADSCs. (b) UMAP plot of lung-originated cell scRNA-seq data, merging cells from the BLM + ADSCs group and BLM + PBS group. Left: dots colored by group. Right: dots colored by SingleR annotated cell type based on clusters identified by Seurat. (c) Stacked violin plot of cluster marker genes (three marker genes for each cluster) and cell count number for each cluster of lung-originated cells.

between injected ADSCs and the PF lung cells (Figure 1(a)) and to improve the understanding of the mechanisms behind the antifibrotic effect of ADSCs.

## 2. Materials and Methods

**2.1. Animals and Experimental Design.** All the animal experiments were conducted under the authorization of the Institutional Animal Care and Use Committee of Tsinghua University. 6-week-old male C57BL/6J male mice, purchased from the Laboratory Animal Research Center of Tsinghua University, were housed in the specific pathogen-free experimental animal environment at the Laboratory Animal Research Center of Tsinghua University, 5~6 mice per cage with sterilized food and water ad libitum and a 12/12-hour light/dark cycle.

**2.2. Isolation of Mouse ADSCs.** 6-week-old C57BL/6J male mouse with body-wide CAG-eGFP expression were obtained from Shanghai Model Organisms Center, Inc. (Shanghai, China). The ADSCs were obtained by euthanizing the mice, digesting their groin adipose tissue with collagenase type I (1.0 mg/ml, Sigma) and cultured in mouse ADSC basal medium (CYAGEN, China) in a humidified atmosphere comprising 5% carbon dioxide at 37°C, according to a previous publication [22].

**2.3. Construction of the BLM-Induced PF Mouse Model and Administration of ADSCs.** The mice were randomly divided into three groups: (i) control group, (ii) BLM + PBS group, and (iii) BLM + ADSCs group.

Groups ii and iii mice were anesthetized with 2.5% tribromoethanol (0.8% NaCl, 1 mM Tris (pH 7.4), 0.25 mM EDTA (pH 7.4)) and administered 3.5 mg/kg bleomycin solution (Sigma B5507-15un) in 50  $\mu$ L of phosphate-buffered saline (PBS) intratracheally on day 0 using a 1 mL syringe with a 25G needle. Control animals were treated with PBS instead of BLM [23, 24].

The injection of ADSCs (at passages 3~6) was performed on day 3 post BLM treatment; 50  $\mu$ L of a cell suspension containing  $1 \times 10^7$  cells/mL in PBS ( $5 \times 10^5$  cells/mouse) was injected intratracheally using a 1 mL disposable syringe with a 25G needle. For the control group and BLM + PBS group, 50  $\mu$ L PBS was injected instead. Before implantation, cells were washed three times to remove the culture medium. The duration of the study was set at four weeks, as the PF remodeling process in mice has been reported to be mostly complete (70~80%) within 3 weeks. All animals were weighed daily from day 0 to 20.

**2.4. Histological Evaluation of Lung Damage and Collagen Deposition of BLM-Induced Lung Injury.** To assess the development of PF, mice were assessed at day 7 and 14. For the

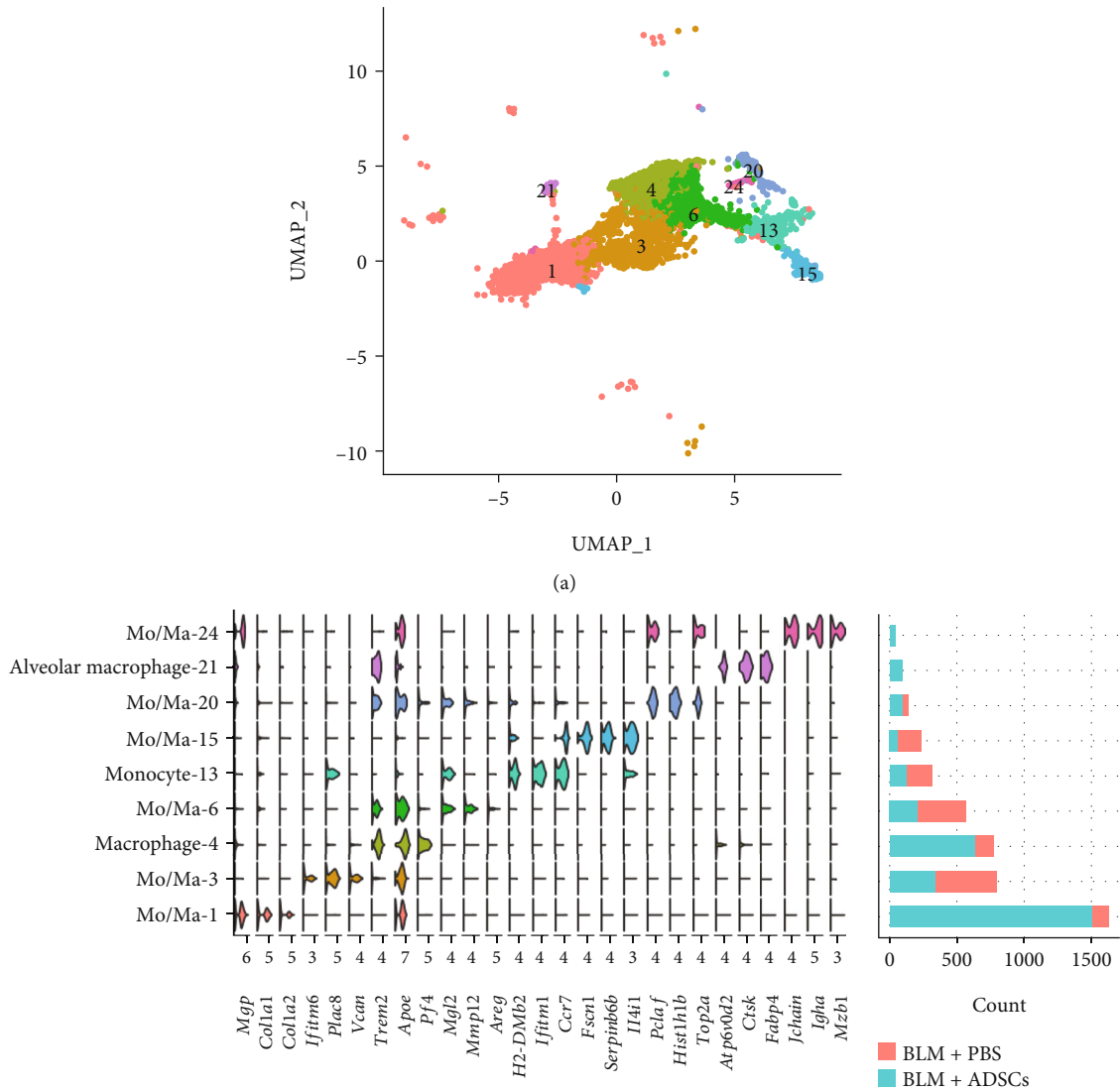
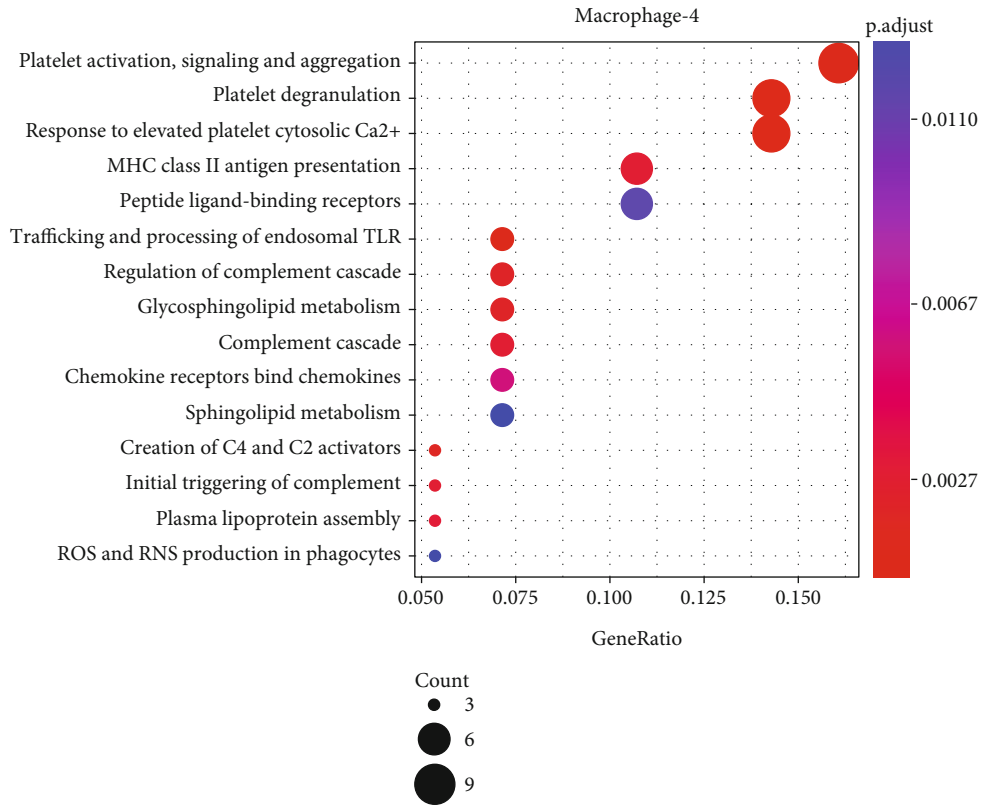
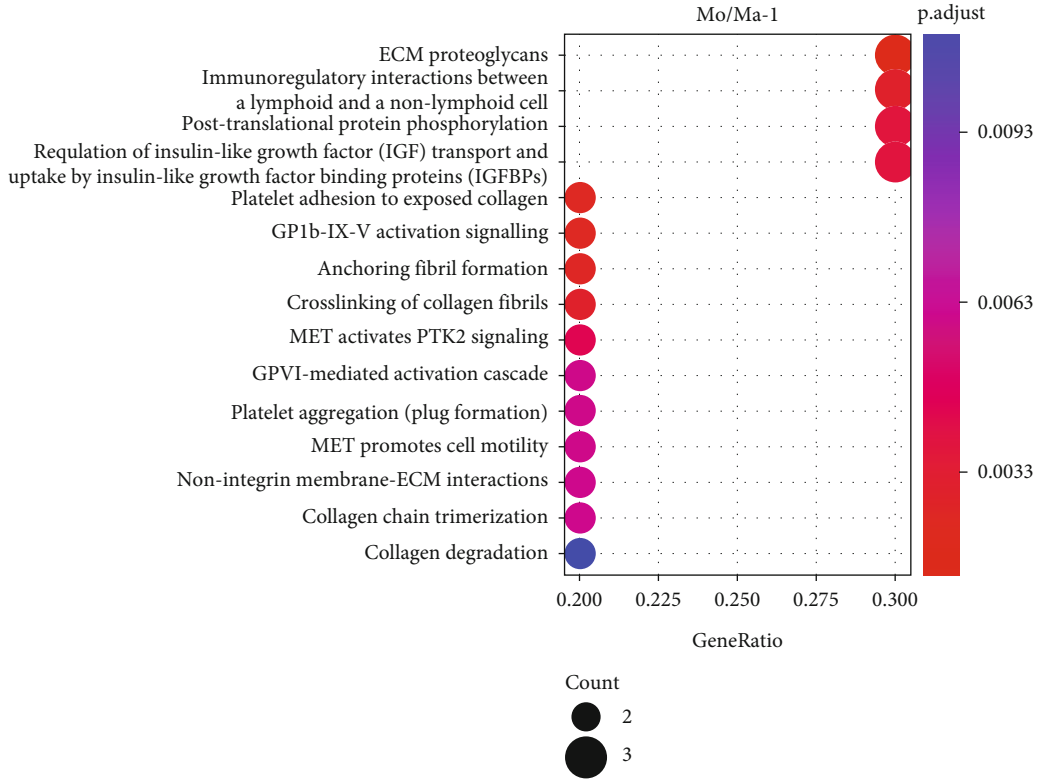


FIGURE 3: Continued.



(c)

FIGURE 3: Continued.

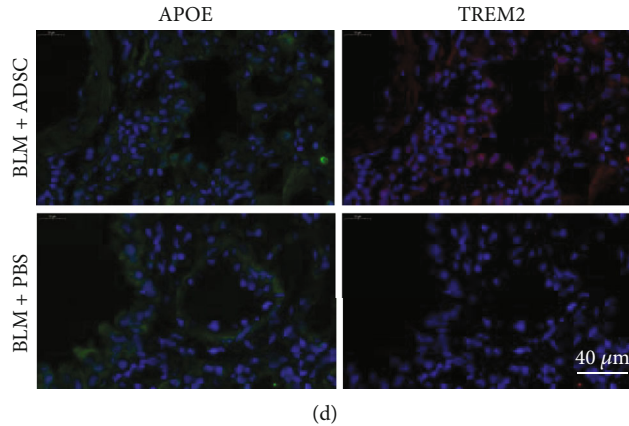


FIGURE 3: ADSC injection changed composition of macrophage population in BLM-treated lung. (a) UMAP distribution of 9 monocyte/macrophage clusters in lung-originated cells, merging the BLM + ADSCs group and BLM + PBS group. (b) Stacked violin plot of cluster marker genes (top three marker genes for each cluster) and cell count of monocyte/macrophage clusters. (c) REACTOME pathway analysis of marker genes of Mo/Ma-1 and macrophage-4 clusters. Genes are filtered by a condition of log<sub>2</sub> fold change >0.5 and adjusted *P* value <0.1. (d) Immunofluorescence images of APOE and TREM2 which the highly expression genes in macrophage-4 on day 7 post BLM treatment.

lung tissue collection, mice were euthanized by CO<sub>2</sub> inhalation. The chest cavity was exposed, and the lungs were perfused and washed with ice-cold PBS. Then, the lungs were fixed with 4% (v/v) paraformaldehyde in PBS and then processed into 5- $\mu$ m-thick paraffin sections mounted on glass slides.

For histological assessment of fibrosis accumulation, slices were stained with hematoxylin and eosin (H&E) or Masson's trichrome stain, respectively. Axio Scan.Z1 (Zeiss, Germany) was used to scan the samples with the 20 $\times$  objective. The images were processed with ZEN 2.3. The lung tissue parenchyma density (alveolar area  $\div$  parenchyma area $\times$ 100%) and fibrosis level (fibrosis area  $\div$  total area $\times$ 100%) were calculated with the Image-Pro premier 3D 9.2.0 using random and non-overlapping fields for grading the lung injury and fibrosis level [25, 26].

**2.5. Preparation of Single-Cell Suspensions.** For the preparation of single-cell suspensions of mouse lung tissue, mice were sacrificed on the 4th day following ADSCs treatment (namely day 7), and the lungs were perfused with PBS. All samples of BLM + ADSCs and BLM + PBS groups were digested using the Lung Dissociation Kit, mouse (130-095-927, Miltenyi Biotec, Germany) according to the manufacturer's instructions. Cells were passed through 70  $\mu$ m and 40  $\mu$ m strainers to remove large pieces, after which the red blood cell lysis solution (Sigma Aldrich, St. Louis, MO, USA) was used to eliminate erythrocytes, followed by flow-assisted cell sorting of pulmonary cells (GFP<sup>-</sup>) and ADSCs (GFP<sup>+</sup>), respectively.

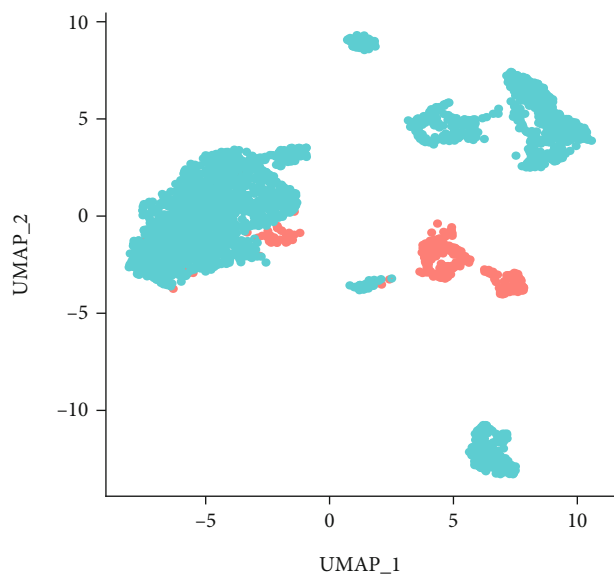
**2.6. Preparation of the scRNA-Seq Library.** We prepared the scRNA-seq libraries using the Chromium Next GEM Single Cell 3' Reagent kit (version 3.1) (10 $\times$  Genomics, USA). Libraries were sequenced on a HiSeq Xten VS NovaSeq 6000 sequencing platform (Illumina, USA), which generated 150 bp paired-end reads.

**2.7. scRNA-Seq Data Processing.** The scRNA-seq library sequences were demultiplexed, mapped to the mouse genome, and counted to generate a gene expression matrix using Cell Ranger (10 $\times$  Genomics). Further data processing was done using the R packages Seurat3 (UMAP visualization, clustering, and gene expression plots), ReactomePA (REACTOME pathway enrichment analysis), and CellChat (cell-cell ligand-receptor interaction analysis).

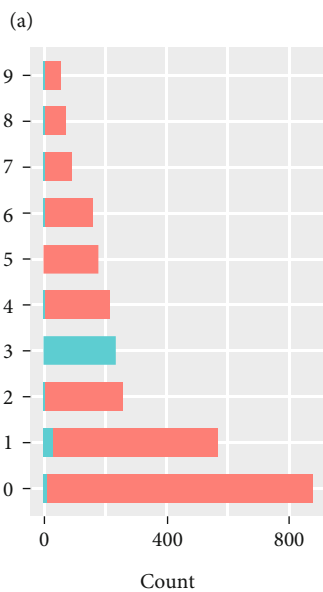
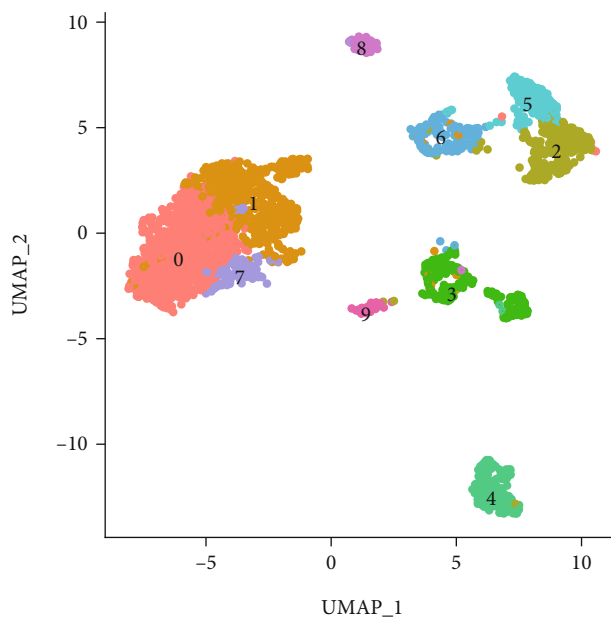
**2.8. Immunofluorescence Staining.** For immunofluorescence staining of APOE and TREM2 in the (ii) BLM + PBS and (iii) BLM + ADSCs groups, mice were anesthetized and lungs were extracted on days 7 and 10. The left lung lobes were fixed with 4% (v/v) paraformaldehyde, paraffin-embedded and cut into 5- $\mu$ m-thick sections. Antibodies were purchased from Biolegend US and immunofluorescence were performed on the sections. The images were scanned using Axio Scan.Z1 and processed with ZEN 2.3.

**2.9. Real-Time Quantitative PCR.** To assess the gene expression levels, mice were euthanized for lung tissue collection and the total RNA was extracted using TRIZOL reagent (Invitrogen, USA) and reverse-transcribed into cDNA using the SuperScript II First-Strand Synthesis System Kit (GenStar, A215, China). The RT-PCR reactions were conducted using 2  $\times$  RealStar Green Fast Mixture (GenStar, A304, China) with 3 technical repeats. *GAPDH* served as the internal reference gene and data were analyzed using the 2 <sup>$-\Delta\Delta$ CT</sup> method. The specific primers were as follows: *TNF- $\alpha$*  (sense, 5'-CAT CTT CTC AAA ATT CGA GTG ACA A-3'; anti-sense, 5'-TGG GAG TAG ACA AGG TAC AAC CC-3'), *IL-1 $\beta$*  (sense, 5'-AGG TCG CTC AGG GTC ACA AG-3'; anti-sense, 5'-GTG CTG CCT AAT GTC CCC TTG AAT C-3'), *IL-10* (sense, 5'-TAA GGC TGG CCA CAC TTG AG-3'; anti-sense, 5'-GTT TTC AGG GAT GAA GCG GC-3'), *IL-6* (sense, 5'-GGT ACA TCC TCG ACG GCA TCT-3'; anti-



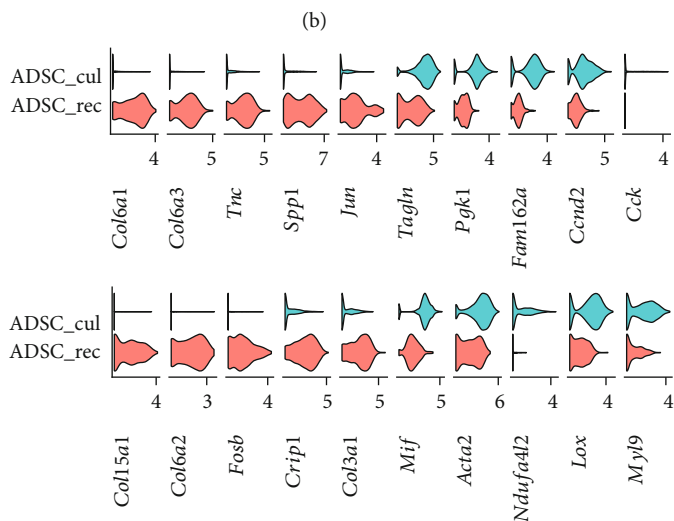


● ADSC\_cul  
● ADSC\_rec



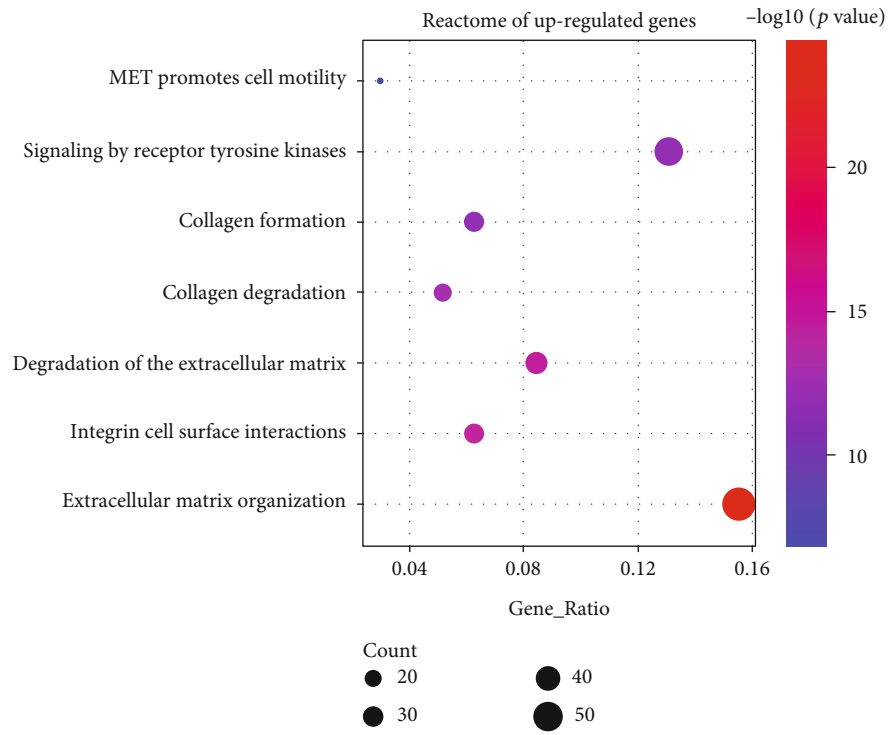
■ ADSC\_cul  
■ ADSC\_rec

(a)

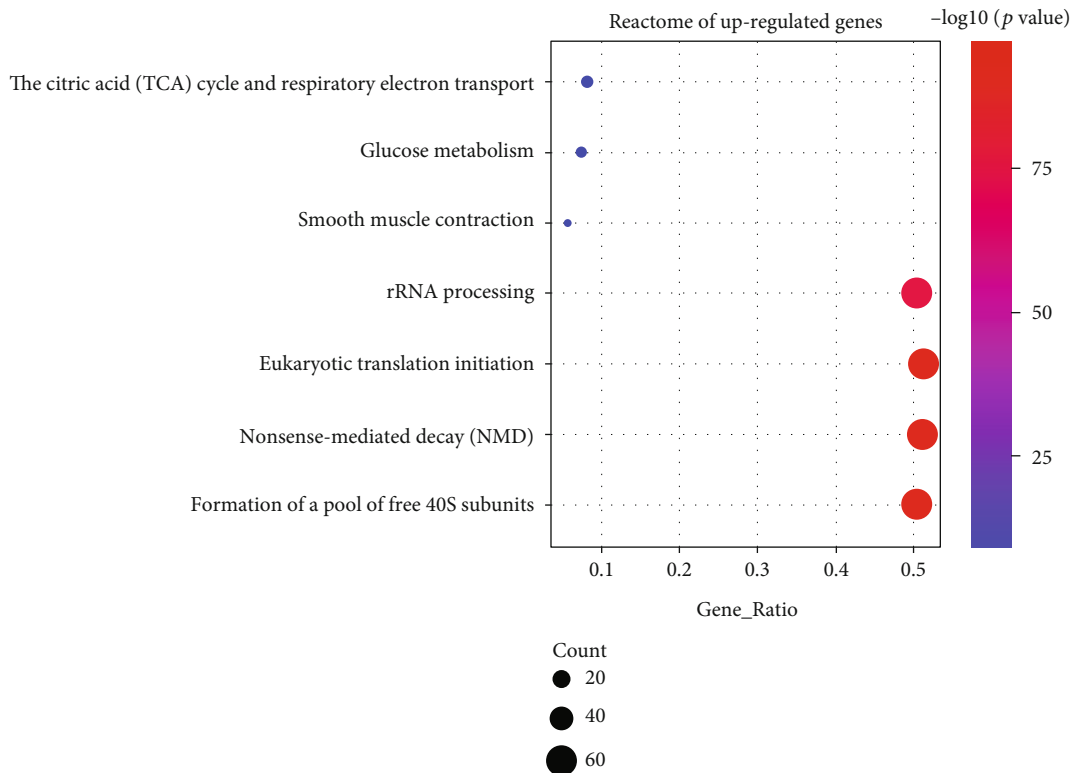


(b)

FIGURE 4: Continued.



(e)



(f)

FIGURE 4: Recollected (ADSC\_rec) ADSCs showed a different single-cell transcriptomic profile compared to cultured ADSCs (ADSC\_cul). (a) UMAP distribution of in vitro cultured (ADSC\_cul) and recollected (ADSC\_rec) ADSCs merged into one dataset. (b) UMAP distribution of all 10 clusters identified by Seurat in merged dataset of ADSC\_cul and ADSC\_rec. (c) Cell count of every cluster in two ADSC groups. (d) Violin plots of differentially expressed genes between ADSC\_cul and ADSC\_rec groups. (e, f) REACTOME pathway enrichment terms of differentially expressed genes ((e) upregulated genes, (f) downregulated genes) in ADSC\_rec group compared to ADSC\_cul group. Genes were first filtered by a condition of  $\log_2$  fold change  $>0.5$  or  $< -0.5$  and adjusted  $P$  value  $<0.05$ .

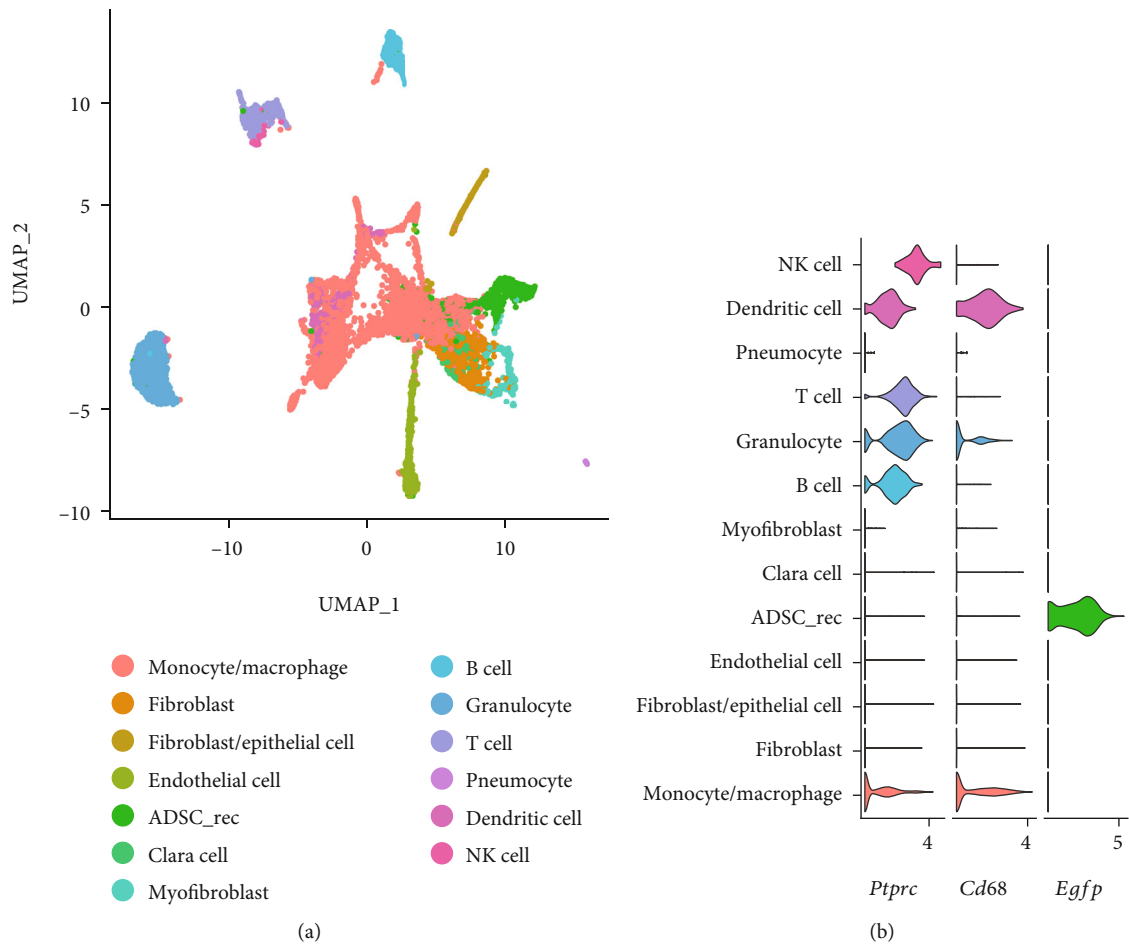
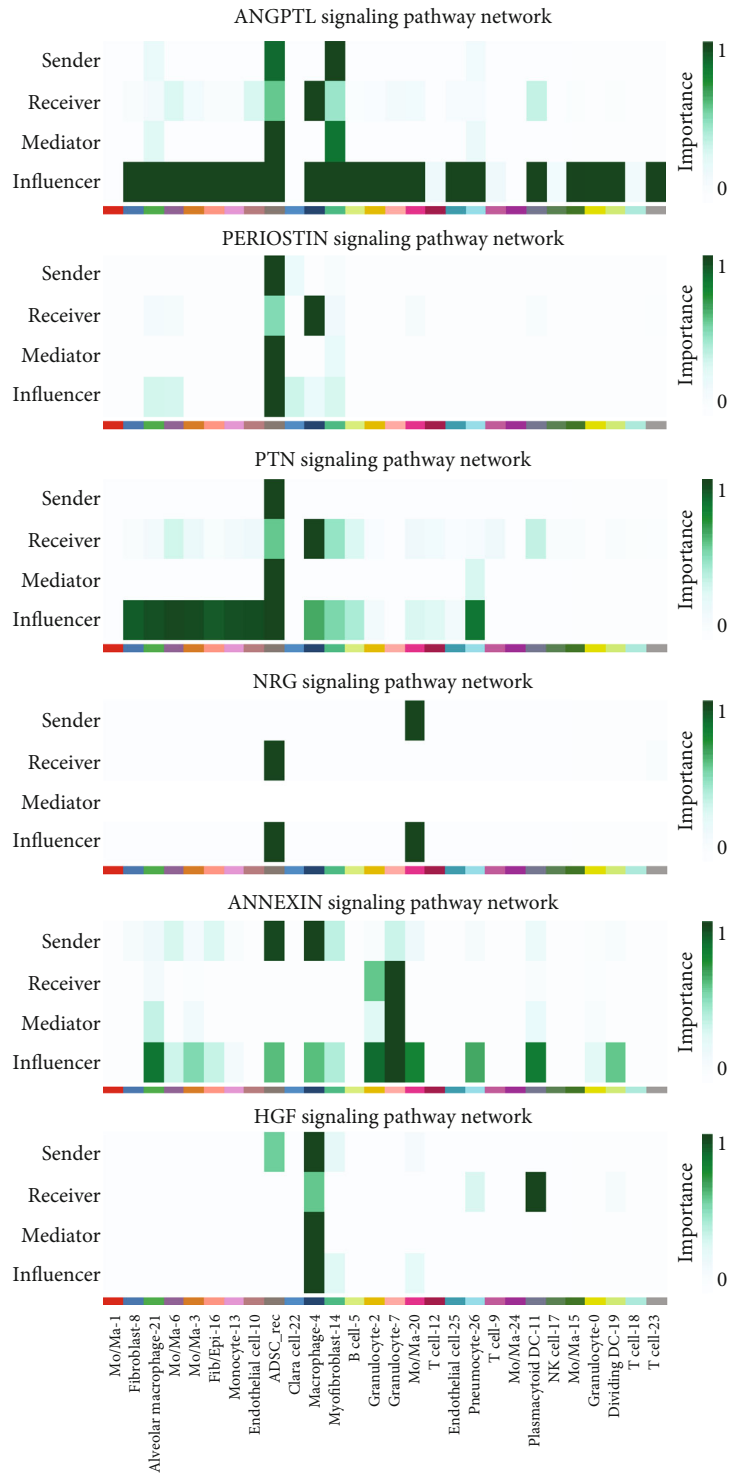


FIGURE 5: Continued.



(c)

FIGURE 5: Continued.

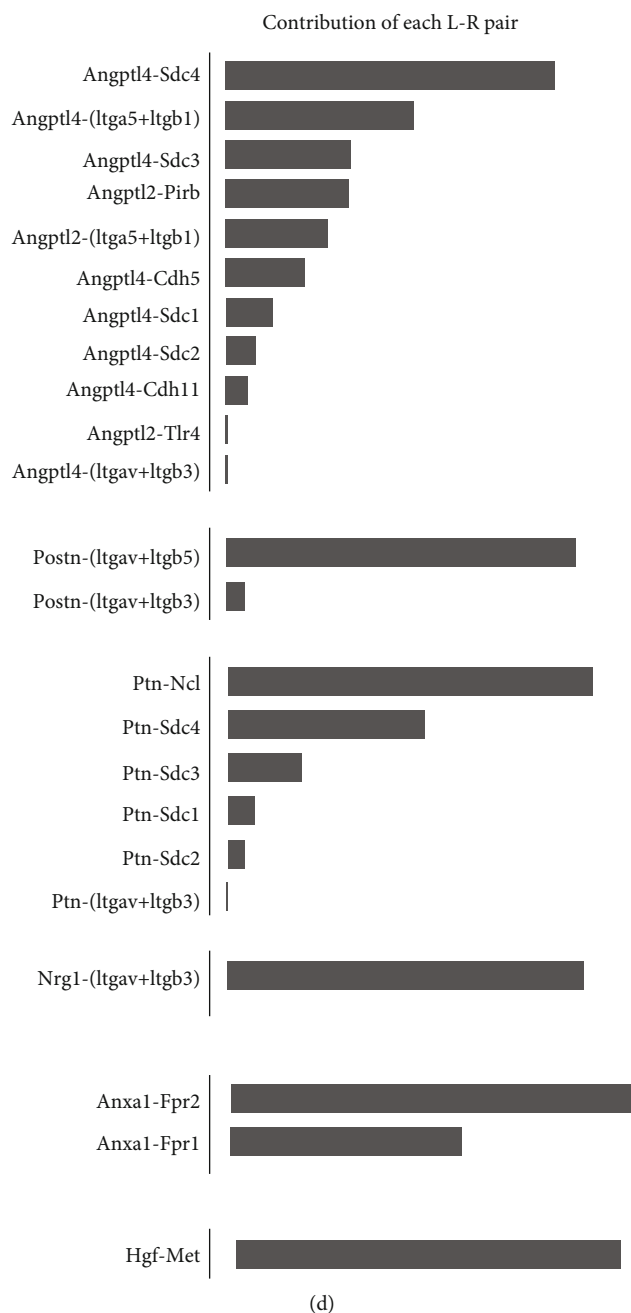


FIGURE 5: CellChat inference of signaling pathways among BLM + ADSCs group. (a) UMAP distribution of coarsely annotated cell type of both lung-originated cells and with recollected ADSCs (ADSC\_rec) in BLM + ADSCs group. (b) Stacked violin plot of Ptprrc (CD45), CD68, and Egfp expression in BLM + ADSCs group. (c, d) Signaling pathway network in BLM + ADSC group calculated by CellChat, showing signaling between recollected ADSCs (ADSC\_rec) and lung-originated cells. (c) Sender, receiver, mediator, and influencer of different pathways. (d) Relative contribution of each ligand-receptor pair in corresponding pathway network.

sense, 5'-GTG CCT CTT TGC TGC TTT CAC-3'), and GAPDH (sense, 5'-GTA GTT GAG GTC AAT GAA GGG-3'; anti-sense, 5'-TCG TCT CAT AGA CAA GAT GGT-3').

2.10. Statistical Analysis. All the experiments were performed in at least three independent replicates, and data are presented as means ± SD and visualized using OriginPro or R software. The statistical significance of differences was

assessed using two-way ANOVA followed by Tukey's multiple comparisons tests (\*P < 0.05; \*\*P < 0.01).

### 3. Results and Discussion

3.1. ADSCs Mitigates PF by Decreasing ECM Deposition and Inflammation. In the BLM-induced PF mouse model, intra-tracheal injection of ADSCs significantly prolonged the survival of the mice in 45 days compared to the BLM + PBS

group (Figure 1(b)). We quantitatively assessed the fibrosis and alveolar damage in the lungs by histological staining, which revealed a visible improvement in the lung texture in the ADSCs group on day 14, though not on day 7 (Figure 1(c)), which were further validated by quantification of the percentage of lung alveolar and fibrotic area (Figures 1(d) and 1(e)). The fibrotic area of the BLM + ADSCs group was 0.4% on day 14, compared to 1.1% in the BLM + PBS group (Figure 1(d)), while the lung alveolar area was  $31.1 \pm 3.1\%$  and  $14.3 \pm 1.3\%$  in the BLM + ADSCs and BLM + PBS group, respectively (control group was  $46.1 \pm 5.5\%$ ) (Figure 1(e)).

Similarly, quantitative real-time PCR showed that the proinflammatory cytokines tumor necrosis factor- $\alpha$  (TNF- $\alpha$ ) and interleukin-1 beta (IL-1 $\beta$ ) were significantly downregulated in the BLM + ADSCs group mouse lungs at days 7 and 14, while antiinflammatory cytokines IL-10 and IL-6 showed the opposite trend (Figure 1(f)). These observations demonstrate that ADSC treatment decreased lung ECM deposition, mitigated fibrosis, and inflammation in mouse PF model.

**3.2. ADSCs Increased the Abundance of antiinflammatory *Trem2*<sup>+</sup> Macrophages in BLM-Treated Lung.** To understand how ADSCs influence the PF environment, we sorted the GFP<sup>+</sup> and GFP<sup>-</sup> cells from the BLM + ADSCs and BLM + PBS groups lung tissue cell suspensions (Figure 2(a)) and then compared single cell profiles of lung-originated (GFP<sup>-</sup>) cells between the BLM + PBS and BLM + ADSCs groups (Figure 2(b)), comprising 8181 and 6405 cells, respectively. A total of 27 cell subgroups were identified in the merged dataset of lung-originated cells (Supplementary Figures 1(a) and 1(b)), and we identified 12 major cell types for each group of lung cells using SingleR (Figures 2(b) and 2(c)).

Among the major cell types, granulocytes were the most abundant in the BLM+PBS group, while monocytes/macrophages were the dominant cell type in the BLM+ADSCs group (Figure 2(c)), indicating drastic inflammation-related changes.

Monocyte/macrophages contained 9 clusters with distinct transcriptomic profiles (Figures 3(a) and 3(b)). The Mo/Ma-1 cluster, characterized by marker genes *MPG*, *COL1a1*, and *SPARC*, was the most abundant population. The macrophage-4 cluster with high expression levels of *APOE* and *TREM2* was the second most abundant (Figure 3(b)). They were both predominantly composed of BLM + ADSCs cells, indicating that they were the potential target and/or effector of with ADSC intervention.

We next examined the function of genes with significant changes of expression levels in the Mo/Ma-1 and macrophage-4 subgroups based on REACTOME pathway analysis. Mo/Ma-1 cluster was related to the regulation of the ECM and proteoglycans, nonintegrin membrane-ECM interactions, collagen chain trimerization, collagen degradation, and crosslinking of collagen fibrils (Figure 3(c)). Macrophage-4 cluster showed higher activity in platelet activation, signaling, aggregation and degranulation, MHC II antigen presentation, and regulation of complement cascade.

It was then determined as *Trem2*<sup>+</sup> macrophages, whose abundance was confirmed to increase at day 7 in the BLM + ADSCs lung tissue, as indicated by the stronger fluorescence signals of TREM2 protein (Figure 3(d)). *TREM2* expression is positively linked to the severity of lung diseases such as viral infection [27] and chronic obstructive pulmonary disease [28], but it is believed to suppress pro-inflammatory responses [27, 29]. The macrophage-4 subgroup therefore might have alleviated the inflammation caused by BLM and ameliorated the subsequent fibrotic response.

**3.3. ADSCs React to BLM-Treated Lung Environment with Dampened Metabolic Activity.** To investigate the potential therapeutic mechanism of intratracheally injected ADSCs in the BLM-treated inflammatory lung microenvironment (BLM + ADSCs group), we analyzed the single-cell transcriptomic profiles of recollected ADSCs from mouse lungs as well as ADSCs cultured *in vitro*. A total of  $1 \times 10^4$  GFP<sup>+</sup> cells from three mice lungs (Figure 2(a)), namely, the recollected ADSCs (ADSC\_rec), were sorted. Together with  $5 \times 10^4$  cultured ADSCs (ADSC\_cul), they were subjected to scRNA-seq, with libraries consisting of 417 cells and 2801 cells, respectively. Unlike the ADSC\_cul group, the ADSC\_rec group does not show much heterogeneity, nor were they similar to any subgroup of ADSC\_cul cells (Figures 4(a)–4(c)), which was likely the result of inadaptability of most cultured ADSCs upon contact with the inflammatory environment in BLM-treated lung. Notably, the ADSC\_rec group showed high expression levels of ECM-related genes like *COL6a1/2/3*, *TNC*, and *COL3a1*, which were hardly expressed by ADSC\_cul cells (Figure 4(d)). We further analyzed the functions of the genes with significant differences between ADSC\_rec and ADSC\_cul ( $\log_2$  fold change  $>0.5$  or  $<-0.5$  and adjusted *P* value  $<0.05$ ) using REACTOME pathway analysis. The upregulated genes of the recollected ADSCs were enriched to REACTOME pathway terms related to extracellular matrix remodeling and cell motility (Figure 4(e)), while their metabolic activity were downregulated as suggested by REACTOME enrichment, including glucose metabolism and RNA processing. (Figure 4(f)).

Recollected ADSCs showed elevated expression of ECM-related genes, while interestingly, histological assessments suggested that ADSCs decreased fibrotic ECM deposition in the lung tissue. It is not likely that injected ADSCs, which only take up a small proportion of ADSC-treated lung cells, was the major contributor of lung ECM reconstruction. And this small population of ADSCs was possibly adhering and adapting to the lung tissue through elevated ECM production compared to their cultured state *in vitro*. In the meantime, the low recollection rate can be explained by the inhibited metabolic activity compared to their cultured counterpart and is another proof that the majority of injected ADSCs cannot permanently reside in the pulmonary tissue, which is unfavorable for the claim that ADSCs transdifferentiate into functional pulmonary cells. Also, the characteristics of recollected subpopulation may provide a hint for improving ADSC survival after injection.

**3.4. ADSCs Crosstalk with Lung-Originated Cells, Especially the *Trem2*<sup>+</sup> Macrophages.** Due to the loss of most injected ADSCs, it is possible that they were gradually engulfed by recipient macrophages. To exclude this complication, we confirmed that the recollected ADSCs do not express *Ptprc* (CD45) or *Cd68* and was the sole subgroup that highly expressed *Egfp* (Figures 5(a) and 5(b)).

To investigate the communication between the injected ADSCs and the lung-originated cells in the BLM-treated lung, we identified the cell-cell interaction with CellChat. The recollected ADSCs mainly received NRG signaling (NRG1-(ITGAV+ITGB3)) from Mo/Ma-20 subgroup (Figures 5(c) and 5(d)). The NRG1-(ITGAV+ITGB3) binding is reported to be essential for NRG1-ERBB signaling [30], which may enhance ADSC migration and resistance to apoptosis [31].

In the meantime, ADSCs affect multiple lung-originated cell subgroups via paracrine signals (Figures 5(c) and 5(d)). The main receiver of ANGPTL, PERIOSTIN, and PTN was macrophage-4, with ANGPTL4-SDC4, POSTN-(ITGAV+ITGB5), and PTN-NCL as the top or sole contributor of ligand-receptor pairs, respectively. ANGPTL4 secreted by MSCs inhibits macrophage proinflammatory polarization [32]. POSTN, however, though reported to promote viability, proliferation, and migration of implanted ADSCs in a hind limb ischemia mice model [33], is also a biomarker and promoter of patient idiopathic PF [34]. PTN pathway plays an important role in fetal lung development and promotes proliferation of type II alveolar cells [35], and PTN protein can induce monocyte-endothelial transdifferentiation [36], but as the top target subgroup of PTN pathway, macrophage-4 yet did not express known endothelial biomarkers such as *Cd34* and *Tie2*. It is possible that these macrophages were also receiving other signals which counteracted or dampened the transdifferentiation-inducing effect of PTN signal.

ADSCs and macrophage-4 interacted with granulocytes-2/7, plasmacytoid dendritic cell (DC)-11, and some monocyte/macrophage subgroups via ANXA1-FPR2 pathway while also affecting macrophage-4 and plasmacytoid DC-11 via HGF. Annexin-A1 (*Anxa1*) counteracts BLM-induced PF [37] and mediates antiinflammatory effects in granulocytic differentiation [38]. HGF has been well studied for its proregenerative role in PF, whose effects include inhibition of epithelial/endothelial cell apoptosis and epithelial-to-mesenchymal transition and facilitation of myofibroblast apoptosis [39]. The macrophage-4 subgroup was the major provider and receiver of HGF signal in ADSC-treated lungs. Macrophage-secreted HGF is reported to promote epithelial repair in Crohn's disease patients, and macrophages under the HGF signal will undergo transition into an anti-inflammatory phenotype in skeletal muscle regeneration [40]. Moreover, plasmacytic DC-11 subgroup is another strong receiver of the HGF signal, and DCs are found to be regulated by MSC-secreted HGF to be immunologically tolerated, which is supportive for alleviating acute lung injury [41]. In our case, these paracrine signals secreted by ADSCs may have played a proregenerative and antiinflammatory role in their encounter with cells in BLM-treated lung, increasing the abundance of *Trem2*<sup>+</sup> macrophage-4 subgroup and further affecting other inflammation-related cell

types including granulocytes and DCs, which orchestrated towards a less inflammatory environment.

Interestingly, our data also suggest that not everything that ADSCs secret may be beneficial for fibrosis resolution, such as POSTN. This could provide potential targets for future precise engineering of ADSCs to weaken their negative effects while enhancing positive ones. And though further explanations need to be made on how cell-cell communication between the injected ADSCs and the damaged lung contribute to mitigating PF, this study represents the first step towards the direct detection of injected cells and understanding their interaction with recipient cells in cell therapy.

## 4. Conclusions

This study is the first to recollect injected ADSCs in mouse PF model and apply scRNA-seq for analysis of interaction between ADSCs and lung-originated cell types. Intratracheally injected ADSCs can alleviate BLM-induced PF, but their number diminishes over time, likely due to dampened metabolic activity, which suggests that ADSCs did not contribute to PF alleviation through transdifferentiation into functional pulmonary cells. Although we only recovered a small fraction of injected ADSCs, and that they did not possess as much heterogeneity as expected, we successfully analyzed the ligand-receptor interactions likely going on in the BLM-treated lung. The remaining ADSCs which were affected by the local NRG signal, through the secretion of effectors like ANGPTL4, HGF, and ANXA1, might have altered macrophages phenotype and influenced DCs to diminish their proinflammatory response. The *Trem2*<sup>+</sup> anti-inflammatory macrophage-4 subgroup was significantly more abundant after ADSCs injection in BLM-treated lungs and was also a major target of multiple ADSC-secreted factors, which is likely the key mechanism through which ADSCs alleviated fibrosis. These results indicated that the injection of ADSCs reduced a proinflammatory response via activating *Trem2*<sup>+</sup> antiinflammatory macrophages in BLM-induced PF. Our work shows the prospect of utilizing scRNA-seq to achieve a perspective closer to the *in vivo* interaction events between injected stem cells and the various types of cells in the disease-challenged tissue, as well as a better understanding towards the mechanisms behind MSC's therapeutic effects.

## Data Availability

The scRNA-seq data used to support the findings of this study are available from the corresponding author upon request.

## Conflicts of Interest

The authors declared no potential conflicts of interest. This manuscript was previously submitted as a pre-print [42].

## Authors' Contributions

M.R., Z.W., and Q.W. initiated this project. J. L. and Q.W. were in charge of supervision. M.R. and Z.W. conducted animal experiments and scRNA-seq. Z.W. performed scRNA-seq data analysis, and M.R. performed qPCR and tissue section staining. H.X. assisted in animal experiments. M.R. and Z.W. prepared this manuscript, and R.W. helped with revision. Mamatali Rahman and Zhao-Yan Wang contributed equally to this work.

## Acknowledgments

This work was supported by the Ministry of Science and Technology of China (Grant No. 2018YFA0900100) and the National Natural Science Foundation of China (Grant Nos. 31961133019, 31670991, and 31470933).

## Supplementary Materials

Supplementary Figure 1: identification of 27 clusters of lung-originated cells in both groups of mice. (*Supplementary Materials*)

## References

- [1] W. A. Wuyts, C. Agostini, K. M. Antoniou et al., "The pathogenesis of pulmonary fibrosis: a moving target," *The European Respiratory Journal*, vol. 41, no. 5, pp. 1207–1218, 2013.
- [2] D. M. Habel and C. Hogaboam, "Heterogeneity in fibroblast proliferation and survival in idiopathic pulmonary fibrosis," *Frontiers in Pharmacology*, vol. 5, p. 2, 2014.
- [3] A. Shah and C. D. Fell, "Idiopathic pulmonary fibrosis: phenotypes and comorbidities," in *Interstitial Lung Disease*, pp. 121–129, 2018.
- [4] D. S. Wilkes, T. Chew, K. R. Flaherty et al., "Oral immunotherapy with type V collagen in idiopathic pulmonary fibrosis," *The European Respiratory Journal*, vol. 45, no. 5, pp. 1393–1402, 2015.
- [5] F. J. Martinez, H. R. Collard, A. Pardo et al., "Idiopathic pulmonary fibrosis," *Nature Reviews. Disease Primers*, vol. 3, no. 1, p. 17074, 2017.
- [6] T. E. King Jr., A. Pardo, and M. Selman, "Idiopathic pulmonary fibrosis," *The Lancet*, vol. 378, no. 9807, pp. 1949–1961, 2011.
- [7] V. L. Kinnula, C. L. Fattman, R. J. Tan, and T. D. Oury, "Oxidative stress in pulmonary fibrosis: a possible role for redox modulatory therapy," *American Journal of Respiratory and Critical Care Medicine*, vol. 172, no. 4, pp. 417–422, 2005.
- [8] K. Rydell-Törmänen, K. Andréasson, R. Hesselstrand et al., "Extracellular matrix alterations and acute inflammation; developing in parallel during early induction of pulmonary fibrosis," *Laboratory investigation*, vol. 92, no. 6, pp. 917–925, 2012.
- [9] S. W. Glasser, J. S. Hagoood, S. Wong, C. A. Taype, S. K. Madala, and W. D. Hardie, "Mechanisms of lung fibrosis resolution," *The American Journal of Pathology*, vol. 186, no. 5, pp. 1066–1077, 2016.
- [10] A. Gazdhar, I. Grad, L. Tamò, M. Gugger, A. Feki, and T. Geiser, "The secretome of induced pluripotent stem cells reduces lung fibrosis in part by hepatocyte growth factor," *Stem Cell Research & Therapy*, vol. 5, no. 6, p. 123, 2014.
- [11] D. Y. Li, R. F. Li, D. X. Sun, D. D. Pu, and Y. H. Zhang, "Mesenchymal stem cell therapy in pulmonary fibrosis: a meta-analysis of preclinical studies," *Stem Cell Research & Therapy*, vol. 12, no. 1, p. 461, 2021.
- [12] J. S. Park, H. N. Yang, D. G. Woo, S. Y. Jeon, and K. H. Park, "The promotion of chondrogenesis, osteogenesis, and adipogenesis of human mesenchymal stem cells by multiple growth factors incorporated into nanosphere-coated microspheres," *Biomaterials*, vol. 32, no. 1, pp. 28–38, 2011.
- [13] K. B. Ackema and J. Charité, "Mesenchymal stem cells from different organs are characterized by distinct topographic Hox codes [in eng]," *Stem Cells and Development*, vol. 17, no. 5, pp. 979–992, 2008.
- [14] S. H. Yu, L. J. Liu, B. Lv et al., "Inhibition of bleomycin-induced pulmonary fibrosis by bone marrow-derived mesenchymal stem cells might be mediated by decreasing MMP9, TIMP-1, INF- $\gamma$  and TGF- $\beta$ ," *Cell Biochemistry and Function*, vol. 33, no. 6, pp. 356–365, 2015.
- [15] K. A. Cieslik, J. Trial, and M. L. Entman, "Aicar treatment reduces interstitial fibrosis in aging mice: suppression of the inflammatory fibroblast," *Journal of Molecular and Cellular Cardiology*, vol. 111, pp. 81–85, 2017.
- [16] Y. Moodley, V. Vaghjani, J. Chan et al., "Anti-inflammatory effects of adult stem cells in sustained lung injury: a comparative study," *Plo S one*, vol. 8, no. 8, article e69299, 2013.
- [17] O. Bernard, F. Jeny, Y. Uzunhan et al., "Mesenchymal stem cells reduce hypoxia-induced apoptosis in alveolar epithelial cells by modulating HIF and ROS hypoxic signaling," *American journal of physiology Lung cellular and molecular physiology*, vol. 314, no. 3, pp. L360–L371, 2018.
- [18] Q. Zhao, C. Hao, J. Wei, R. Huang, C. Li, and W. Yao, "Bone marrow-derived mesenchymal stem cells attenuate silica-induced pulmonary fibrosis by inhibiting apoptosis and pyroptosis but not autophagy in rats [in eng]," *Ecotoxicology and Environmental Safety*, vol. 216, article 112181, 2021.
- [19] E. Ivanova-Todorova, I. Bochev, M. Mourdjeva et al., "Adipose tissue-derived mesenchymal stem cells are more potent suppressors of dendritic cells differentiation compared to bone marrow-derived mesenchymal stem cells," *Immunology Letters*, vol. 126, no. 1-2, pp. 37–42, 2009.
- [20] D. Noël, D. Caton, S. Roche et al., "Cell specific differences between human adipose-derived and mesenchymal-stromal cells despite similar differentiation potentials," *Experimental Cell Research*, vol. 314, no. 7, pp. 1575–1584, 2008.
- [21] A. Moya, J. Paquet, M. Deschepper et al., "Human mesenchymal stem cell failure to adapt to glucose shortage and rapidly use intracellular energy reserves through glycolysis explains poor cell survival after implantation," *Stem Cells*, vol. 36, no. 3, pp. 363–376, 2018.
- [22] J. Qian, Y. Hu, L. Zhao et al., "Protective role of adipose-derived stem cells in Staphylococcus aureus-induced lung injury is mediated by Reg IIIgamma secretion," *Stem cells*, vol. 34, no. 7, pp. 1947–1956, 2016.
- [23] P. Llontop, D. Lopez-Fernandez, B. Clavo et al., "Airway transplantation of adipose stem cells protects against bleomycin-induced pulmonary fibrosis," *Journal of investigative medicine: the official publication of the American Federation for Clinical Research*, vol. 66, no. 4, pp. 739–746, 2018.
- [24] A. Tzouvelekis, G. Koliakos, P. Ntoliou et al., "Stem cell therapy for idiopathic pulmonary fibrosis: a protocol proposal," *Journal of Translational Medicine*, vol. 9, no. 1, p. 182, 2011.



- [25] S. R. Boser, T. Mauad, B. B. Araújo-Paulino et al., "Myofibroblasts are increased in the lung parenchyma in asthma," *PLoS One*, vol. 12, no. 8, article e0182378, 2017.
- [26] J. A. Jerome, S. E. Wenzel, and H. E. Trejo Bittar, "Digital imaging analysis reveals reduced alveolar  $\alpha$ -smooth muscle actin expression in severe asthma," *Applied immunohistochemistry & molecular morphology: AIMM*, vol. 29, no. 7, pp. 506–512, 2021.
- [27] Z. Zhu, X. Zhang, W. Dong et al., "TREM2 suppresses the pro-inflammatory response to facilitate PRRSV infection via PI3K/NF- $\kappa$ B signaling," *PLoS Pathogens*, vol. 16, no. 5, article e1008543, 2020.
- [28] D. E. Byers, K. Wu, G. Dang-Vu et al., "Triggering receptor expressed on myeloid cells-2 expression tracks with M2-like macrophage activity and disease severity in COPD [in eng]," *Chest*, vol. 153, no. 1, pp. 77–86, 2018.
- [29] I. R. Turnbull, S. Gilfillan, M. Cella et al., "Cutting edge: TREM-2 attenuates macrophage activation," *Journal of immunology*, vol. 177, no. 6, pp. 3520–3524, 2006.
- [30] K. Ieguchi, M. Fujita, Z. Ma et al., "Direct binding of the EGF-like domain of neuregulin-1 to integrins ( $\alpha$ v $\beta$ 3 and  $\alpha$ 6 $\beta$ 4) is involved in neuregulin-1/Erb B signaling [in eng]," *The Journal of Biological Chemistry*, vol. 285, no. 41, pp. 31388–31398, 2010.
- [31] X. Liang, Y. Ding, Y. Zhang et al., "Activation of NRG1-ERBB4 signaling potentiates mesenchymal stem cell-mediated myocardial repairs following myocardial infarction [in eng]," *Cell Death & Disease*, vol. 6, no. 5, p. e1765, 2015.
- [32] D. I. Cho, H.-j. Kang, J. H. Jeon et al., "Antiinflammatory activity of ANGPTL4 facilitates macrophage polarization to induce cardiac repair," *Insight*, vol. 4, no. 16, 2019.
- [33] J. Qin, F. Yuan, Z. Peng et al., "Periostin enhances adipose-derived stem cell adhesion, migration, and therapeutic efficiency in Apo E deficient mice with hind limb ischemia," *Stem Cell Research & Therapy*, vol. 6, no. 1, p. 138, 2015.
- [34] P. K. Naik, P. D. Bozyk, J. K. Bentley et al., "Periostin promotes fibrosis and predicts progression in patients with idiopathic pulmonary fibrosis," *American Journal of Physiology-Lung Cellular and Molecular Physiology*, vol. 303, no. 12, pp. L1046–L1056, 2012.
- [35] T. Weng, L. Gao, M. Bhaskaran et al., "Pleiotrophin regulates lung epithelial cell proliferation and differentiation during fetal lung development via  $\beta$ -catenin and Dlk1," *Journal of Biological Chemistry*, vol. 284, no. 41, pp. 28021–28032, 2009.
- [36] B. G. Sharifi, Z. Zeng, L. Wang et al., "Pleiotrophin induces transdifferentiation of monocytes into functional endothelial cells," *Arteriosclerosis, Thrombosis, and Vascular Biology*, vol. 26, no. 6, pp. 1273–1280, 2006.
- [37] A. S. Damazo, A. L. F. Sampaio, C. M. A. G. Nakata, R. J. Flower, M. Perretti, and S. M. Olini, "Endogenous annexin A1 counter-regulates bleomycin-induced lung fibrosis," *BMC Immunology*, vol. 12, no. 1, p. 59, 2011.
- [38] W. H. Tsai, H. Y. Chien, C. H. Shih et al., "Annexin A1 mediates the anti-inflammatory effects during the granulocytic differentiation process in all-trans retinoic acid-treated acute promyelocytic leukemic cells [in eng]," *Journal of Cellular Physiology*, vol. 227, no. 11, pp. 3661–3669, 2012.
- [39] B. Crestani, S. Marchand-Adam, C. Quesnel et al., "Hepatocyte growth factor and lung fibrosis," *Proceedings of the American Thoracic Society*, vol. 9, no. 3, pp. 158–163, 2012.
- [40] W. Choi, J. Lee, J. Lee, S. H. Lee, and S. Kim, "Hepatocyte growth factor regulates macrophage transition to the M2 phenotype and promotes murine skeletal muscle regeneration," *Frontiers in Physiology*, vol. 10, pp. 914–914, 2019.
- [41] Z. Lu, W. Chang, S. Meng et al., "Mesenchymal stem cells induce dendritic cell immune tolerance via paracrine hepatocyte growth factor to alleviate acute lung injury," *Stem Cell Research & Therapy*, vol. 10, no. 1, p. 372, 2019.
- [42] M. Rahman, Z. Y. Wang, J. X. Li, H. W. Xu, and Q. Wu, *Single-cell RNA sequencing reveals that injected ADSCs change the macrophage profile in a murine model of pulmonary fibrosis*, Research Square, 2021.